Ocean Dynamics
DOI 10.1007/s10236-016-1021-4

An investigation into the dispersion of ocean surface waves in sea ice

Clarence Olin Collins III[1] · **William Erick Rogers**[1] · **Björn Lund**[2]

Received: 29 February 2016 / Accepted: 20 November 2016

Abstract This investigation considers theoretical models and empirical studies related to the dispersion of ocean surface gravity waves propagating in ice covered seas. In theory, wave dispersion is related to the mechanical nature of the ice. The change of normalized wavenumber is shown for four different dispersion models: the mass-loading model, an elastic plate model, an elastic plate model extended to include dissipation, and a viscous-layer model. For each dispersion model, model parameters are varied showing the dependence of deviation from open water dispersion on ice thickness, elasticity, and viscosity. In all cases, the deviation of wavenumber from the open water relation is more pronounced for higher frequencies. The effect of mass loading, a component of all dispersion models, tends to shorten the wavelength. The Voigt model of dissipation in an elastic plate model does not change the wavelength. Elasticity in the elastic plate model and viscosity in the viscous-layer model tend to increase the wavelength. The net effect, lengthening or shortening, is a function of the particular combination of ice parameters and wave frequency. Empirical results were compiled and interpreted in the context of these theoretical models of dispersion. A synopsis of previous measurements is as follows: observations in a loose pancake ice in the marginal ice zone, often, though not always, showed shortened wavelengths. Both lengthening and shortening have been observed in compact pancakes and pancakes in brash ice. Quantitative matches to the flexural-gravity model have been found in Arctic interior pack ice and sheets of fast ice.

Keywords Dispersion · Ocean surface waves · Sea ice · Marginal ice zone · Attenuation · Flexural-gravity waves · Snell's law · Wavelength · Viscosity · Shear modulus · Elastic modulus · SAR · Marine radar · Buoy measurements

1 Introduction

With enough time and space, the action of wind at the air-sea interface will induce gravity waves (henceforth waves) which propagate across the surface of the seas. Waves may propagate into, and interact with, regions of partial or complete ice cover. Ice may be in the form of slurry, a continuous sheet, floes of various sizes and arrangements, or any combination these.

Wave prediction is of utmost importance for the safety of operations, but in the polar oceans, due to the presence of ice and the resulting wave-ice interaction, wave prediction is problematic. The interaction is a two-way coupled problem: ice not only affects waves, but waves affect ice. In the Arctic, wave action and ice cover may be connected via feedback loop where waves fracture ice; the ice melt is enhanced due to an increased lateral surface area, and a larger fetch is available for wave development (Asplin et al. 2012; Asplin et al. 2014). Hence, wave-ice interaction is an important physical process that may, in part, determine the fate of sea ice extent as the Arctic warms (Thomson and Rogers 2014; Thomson et al. 2016).

This article is part of the Topical Collection on *the 14th International Workshop on Wave Hindcasting and Forecasting in Key West, Florida, USA, November 8–13, 2015*

Responsible Editor: Oyvind Breivik

✉ Clarence Olin Collins, III
Tripp.Collins@nrlssc.navy.mil

[1] US Naval Research Laboratory, Oceanography Division, 1005 Balch Blvd, Stennis Space Center, Hancock County, MS 39529, USA

[2] Department of Ocean Sciences, University of Miami, Rosenstiel School of Marine and Atmospheric Science, Miami, FL, USA

Published online: 14 December 2016

The one-way interactions of this coupled process can be described in simple terms. Waves to ice: waves stress and potentially fracture ice. Ice to waves: ice refracts, shoals, and attenuates waves—the latter is an outcome of dissipation, reflection, and scattering. In the complex formulation of the wavenumber in the dispersion relation, the real part is related to the change in wavelength, and the imaginary part to attenuation due to dissipation. The majority of previous studies have focused on attenuation because the phenomenon is relatively easy to measure, and therefore has been well documented (e.g., Squire and Moore (1980), Wadhams et al. (1988), Squire et al. (1995), Squire (2007). There is some agreement on the order of magnitude of attenuation, but little consensus on whether the dominant mechanisms are related to scattering or dissipation (covering a number or proposed physical mechanisms). Although comprehensive measurements of in-ice dispersion have yet to be achieved, it is anticipated that these will be available in the near future, possibly from the recent Office of Naval Research (ONR) "Sea State and Boundary Layer Physics of the Emerging Arctic Ocean" (Sea State) research initiative (Thomson et al. 2013).[1] Therefore, this study explores features of the much less-studied, real part of dispersion or, in other words, the change in wavenumber.

Dispersion refers to the fact that (in intermediate and deep waters) waves of different frequencies propagate at different speeds, and so "disperse" in space and time (e.g., Snodgrass et al. 1966), and it is this dispersion relation which connects temporal and spatial wave kinematics.

Immediately upon entering icy seas, wave dispersion is altered from the open water relation. This change from the open water dispersion relation results in an altered wavelength, phase velocity, direction, group velocity, and wave height, but the frequency and action (i.e., energy divided by frequency) are invariant. After propagating some distance in ice, wave height decreases due to attenuation.

The open water dispersion relationship is derivable from first principles: Newton's 2nd law for body forces on a fluid continuum manifests as the Navier-Stokes equation. Assumptions are made about water so that several terms in the Navier-Stokes equation are negligible. This includes neglecting viscosity (it is later included in a 2-layer in-ice model), neglecting compressibility, and assuming water motion is irrotational. If water is assumed to be incompressible and irrotational, the fluid velocity can be described by the gradient of a scalar function called the velocity potential. The dynamic boundary conditions at the interface require the normal stress to be continuous and the shear stress to vanish (for an inviscid water surface). Detailed derivations are available in the literature (e.g., Kinsman (1965)).

[1] http://www.apl.washington.edu/project/project.php?id=arctic_sea_state

By linearizing the dynamic boundary condition at the surface, the open water (i.e., ice free) dispersion relation is:

$$\omega = \sqrt{gk \tanh kd} \tag{1}$$

where ω is the wave frequency, k is the wavenumber, d is the water depth, and g is the acceleration due to gravity. The wavelength is $2\pi/k$. For simplicity, Eq. (1) is taken to the deep water limit, such that $\tanh(kd)$ approaches 1:

$$\omega = \sqrt{gk} \Leftrightarrow \frac{\omega^2}{g} = k \equiv k_{ow} \tag{2}$$

Here, k_{ow} is defined as the open water wavenumber. The deep water limit is maintained throughout the remainder of this study, though intermediate-depth forms are available in general.

The mechanical model of the ice determines the stress-strain relationships which are enforced in the boundary conditions, and the boundary conditions alter the form of the dispersion relation derived from a potential flow theory (e.g., Mosig et al. 2015). In the forthcoming sections, the open water dispersion relation—Eq. (2)—will be progressively complicated by introducing extra terms. The most basic formulation, and a component in all subsequent models, is a term due to the added inertia of ice on the surface (Section 2.1). Under the umbrella of ice as an elastic plate, a term due to elastic response to wave-induced bending is introduced (Section 2.2.1), then a note on compression (Section 2.2.2), and finally the addition of dissipation (Section 2.2.3). A different approach is then introduced: the viscous-layer model (Section 2.3). With each model, idealized ice conditions are described which would be the most appropriate for the application of that particular model. Given the in-ice dispersion relation, Snell's law is used to derive the expected shoaling and refraction (Section 3). This is followed by a survey of the previous field and laboratory measurements of dispersion (Section 4). The article ends with a discussion (Section 5) which focuses on dispersion models and their implementation in spectral wave models (Section 5.1), measurement deficiencies (Section 5.2), a picture of the status quo (Section 5.3), future prospects (Section 5.4), and ice and unresolved processes (Section 5.5).

Recent descriptions of wave-induced ice-fracture events (Asplin et al. 2012; Kohout et al. 2014; Collins et al. 2015; Kohout et al. 2015) led to a deceptively simple question: do open water surface waves increase or decrease their height immediately upon entering ice, potentially increasing or decreasing the expected stress delivered to the ice? According to Snell's law, this question is exactly the same as asking: does the dispersion relation change? This investigation is the result of exploring this question.

The literature on wave-ice interaction and ice mechanics is enormously rich and growing. For those familiar with surface

wave mechanics, it is hoped that this study will act as an introduction and a bridge to the more sophisticated treatments given in Mosig et al. (2015) and Zhao et al. (2015), for example. For broad reviews, please see Squire et al. (1995), Wadhams (2000), Squire (2007), and Collins et al. (2016).

2 Theoretical wave dispersion in ice

2.1 Mass-loading model

The simplest way to introduce the effects of ice on wave dispersion is by including the added mass of ice at the interface. This is known as the mass-loading model.[2] The mass loading model (ML) may be appropriate for conditions where the wavelength is much longer than the typical ice floe length such that there is no elastic response of ice, and adjacent floes do not interact. For example, long swell propagating through small (compared to the characteristic wavelength), sparsely spaced or noninteracting ice floes. This type of ice can occur within the marginal ice zone (MIZ) either as broken floes or as pancakes.[3] The ML model was originally developed in the 1950s (see Weitz and Keller (1950) and the discussion within Squire et al. (1995)); the resulting dispersion relation is

$$\frac{\omega^2}{g - \rho_{ice} h \omega^2 / \rho} = k \tag{3}$$

ρ is the familiar water density and ice is introduced through the inclusion of ice density, ρ_{ice}, and thickness, h. Ice concentration, c, a scalar representing the fraction of surface area covered by ice, may be written into the equation explicitly:

$$\frac{\omega^2}{g - c\rho_{ice} h \omega^2 / \rho} = k \tag{4}$$

following Liu and Mollo-Christensen (1988), the presentation can be simplified by defining an inertial coefficient, M:

$$\frac{\omega^2}{g - M\omega^2} = k \tag{5}$$

it is worth noting that M represents inertia of ice below the mean water level as ice can also have some freeboard, i.e., volume above the mean water level. In Fig. 1, the density of seawater was set as 1025 kg m^{-3}, ρ_{ice} was set to 90% of ρ, and c is 100%. There is only one free parameter, h, and as the h approaches zero, the inertial term in the denominator approaches zero and Eq. (5) simplifies to that of open, deep water relationship of Eq. (2).

The effect of different ice thicknesses on the dispersion relation is shown in Fig. 1. The wavenumber was normalized by the open water wavenumber, k_{ow}, so that the y-axis is the deviation from the open water relation. Figure 1 shows that the mass loading model (1) always increases the wavenumber (shortens the wavelength) and (2) that deviation from open water wavenumber is greater as the frequency increases. Even for a relatively thin ice, h = 0.21 m, the wavenumber corresponding to 0.8 Hz is double that of the open water relationship. For long waves, f < 0.1 Hz, the relative effect of ice of 3.5 m thick is less substantial, e.g., a 15% increase in wavenumber at 0.10 Hz.

Many of the lines asymptote at a particular frequency, implying a high frequency limit. Indeed, it is clear from Eq. (5) that as $k \to \infty$ the denominator approaches zero and wave frequency approaches the following limit

$$\omega \to \omega_c = 2\pi f_c = \sqrt{\frac{\rho g}{\rho_{ice} c h}} \tag{6}$$

(Wadhams and Holt 1991). Waves with open water frequencies above this limit are completely reflected and do not enter the ice as the reflection coefficient is $|R| = |k_{ice} - k_{ow}|/(k_{ice} + k_{ow})$ for normally incident waves (Keller and Weitz, 1953).

2.2 Elastic plates

2.2.1 Pure elastic plate

The dynamic free surface boundary condition states that the pressure just below the free surface is equal to the ambient (air-side) pressure; without ice, this results to the Bernoulli equation. In ice, an additional pressure term comes from the volumetric stress in ice. The stress-strain relationship is dictated by the model chosen for the mechanical behavior of ice.

Here, ice is modeled as a thin, elastic plate in which surface waves induce coupled wave modes. For this model to be appropriate, the typical size of ice floes should be much larger than the characteristic wavelength. Though academic in concept, a near approximation would be a uniform ice layer which form naturally as fast ice in fjords, harbors, and inlets. For very low frequencies (0.03–0.05 Hz), the central pack ice in the Arctic may approximate a uniform sheet.

Re-deriving the dispersion relation, the material property of flexural-rigidity, L, shows up in the denominator as a term proportional to k^4.

$$\frac{\omega^2}{g - M\omega^2 + Lk^4/\rho} = k \tag{7}$$

[2] Also referred to as "added mass" model, the "inertial" model, the "added inertia" model, and possibly others.

[3] Unfamiliar with basic ice types? Please see http://seaiceatlas.snap.uaf.edu/glossary for detailed definitions. Ice types mentioned in this manuscript are pancake, frazil, brash, grease, pack ice, and fast ice sheets.

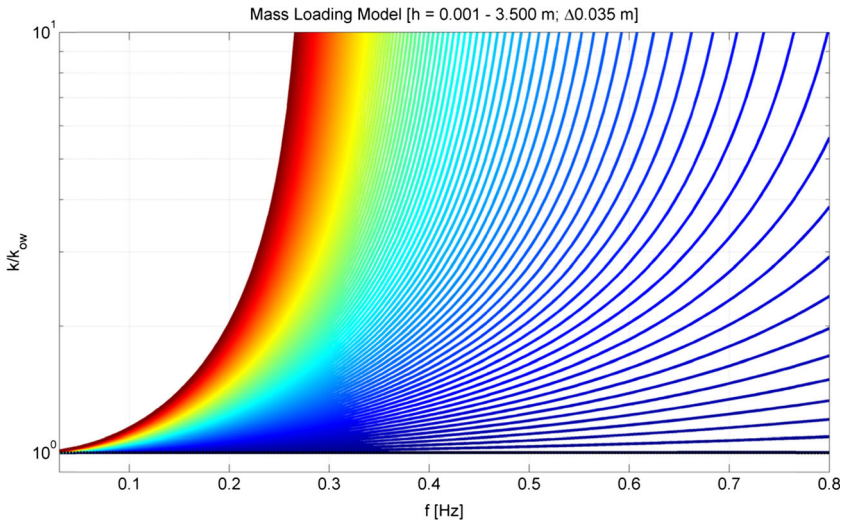

Fig. 1 The normalized dispersion relation calculated from the mass loading model as a function of ice thickness, h. The thickness ranges from 0.001 to 3.500 m linearly (Δh = 0.035 m) where h = 0 is the deep water linear dispersion relation shown by the *black line* and h = 3.5 m is the *dark red line*

A simple mechanical model is an application of the Euler-Bernoulli beam theory or its extension, Kirchoff-Love plate theory (Fox and Squire 1994) (FS) where the flexural-rigidity of the sea ice is a function of three ice parameters (1) the thickness, h, (2) the effective elastic modulus, Y, and (3) the Poisson ratio, v:

$$L \equiv \frac{Yh^3}{12(1-\nu^2)} \tag{8}$$

In this case, ice is purely elastic (linear strain response to stress). The elastic modulus (Y) and shear modulus (G) are Lamé constants with simple relations (Wang and Shen 2010a):

In the following example, the free parameter is chosen to be G and ν is set to 0.3.

$$Y = 2G(1+\nu) \tag{9}$$

$$\nu = \frac{Y}{2G} - 1 \tag{10}$$

The elastic term tends to increase wavelength (Squire 1993). According to Fig. 2, whether the wave shortens or lengthens depends on the relative contributions of the inertial and elastic terms in the demoninator. When the shear modulus approaches zero, then the mass loading Eq. (5) is recovered from Eq. (7).

The frequency at which the dominant term transitions to elastic term is given by Fox and Haskell (2001):

$$\omega_t = 2\pi f_t = \left(\frac{\rho g^5}{L}\right)^{\frac{1}{8}} \tag{11}$$

Figure 2 shows that a 0.1 Hz wave is significantly lengthened, but only for combinations of thick h and large G. Otherwise, the ML term dominates and the wavenumber tends to increase.

Figure 3 shows the relative change in wavenumber for a 0.1-Hz wave as a function of G for a given ice thickness. For the thicknesses tested, deviations from the ML model slowly appear beyond a shear modulus of 10^6 Pa. For a given h, after the effects of elasticity appear, the wavelength rapidly increases as a function of G (and h). For the same level of shear modulus, say 10^{10} Pa, a change in ice thickness from 1 to 2 m leads to a change in a wavelength of ~60 m.

2.2.2 Elastic plate with compression

Motivated by an ice-fracture event, Liu and Mollo-Christensen (1988) formulated the effects of compressive stress into the elastic plate model:

$$\frac{\omega^2}{g - M\omega^2 + Bk^4 - Phk^2/\rho} = k \tag{12}$$

where the bending coefficient, $B = L/\rho$ is introduced with P being the compressive stress. This can be further simplified by defining a compressive coefficient, $Q = Ph/\rho$

$$\frac{\omega^2}{g - M\omega^2 + Bk^4 - Qk^2} = k \tag{13}$$

There is an analogy between compressive stresses in a wave dispersion with the effects of surface tension, the equation for which bears the form:

$$\omega^2 = \left(gk + \frac{Tk^3}{\rho}\right)\tanh kd \tag{14}$$

where T is the surface tension of water. By taking this form to the deep water limit, and rearranging:

$$\frac{\omega^2}{g + Tk^2/\rho} = k \tag{15}$$

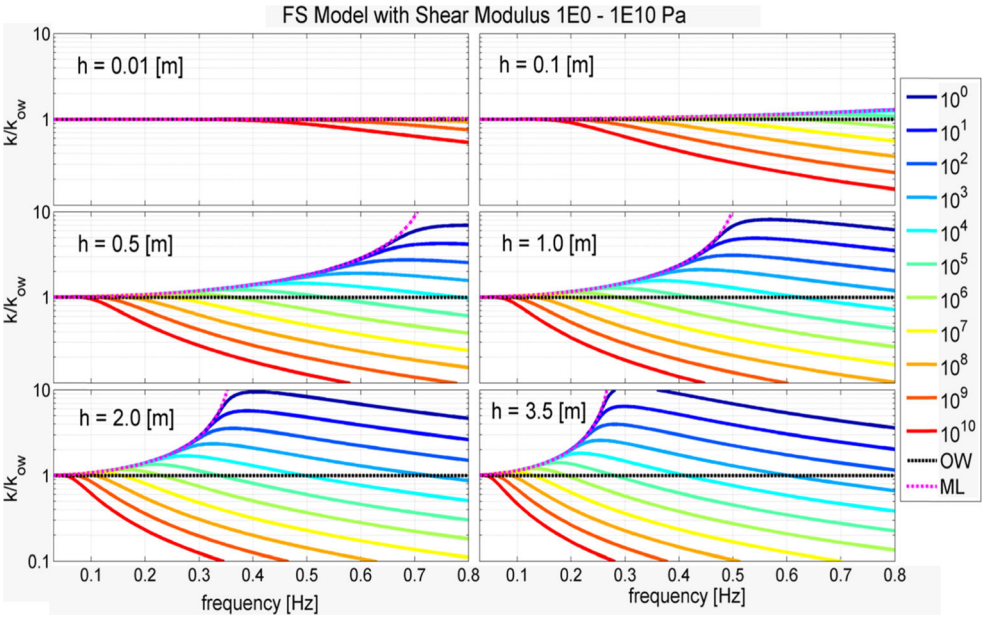

Fig. 2 The normalized wavenumber from the pure elastic plate model with shear modulus, *G,* varying over 11 decades from 1 Pa (dark blue) to 10^{10} Pa (dark red). Ice thicknesses of 0.01, 0.1, 0.5, 1.0, 2.0, and 3.5 m are shown in seperate panels from left to right, top to bottom, respectively

now, the surface tension, T, and the compressive stress can be related by the following equation:

$$P = -T/h \tag{16}$$

So, compressive stress acts like a negative surface tension scaled by the ice thickness. The effect of compressive stress is to increase the wavenumber (see Fig. 1a of Liu and Mollo-Christensen (1988)), but the compressive stress assumed, 5.1×10^6 Nm^{-2}, is considered unrealistic under most conditions (Timco and Weeks 2010). However, it is conceivable that situations occur that increase compressive stress within ice cover, such as a strong on-ice storm event in which the ice edge becomes compact due to wave and wind forcing, and inclusion of the compressive stress term may need to be considered.

2.2.3 Elastic plate with dissipation

Observations have shown that wave energy attenuates exponentially as a function of propagation distance into ice (Wadhams et al. 1988). This attenuation may be due to the energy conserving process of wave reflection and scattering (e.g., Kohout and Meylan (2008)) or any number of nonconservative, dissipative processes. Here, dissipation is

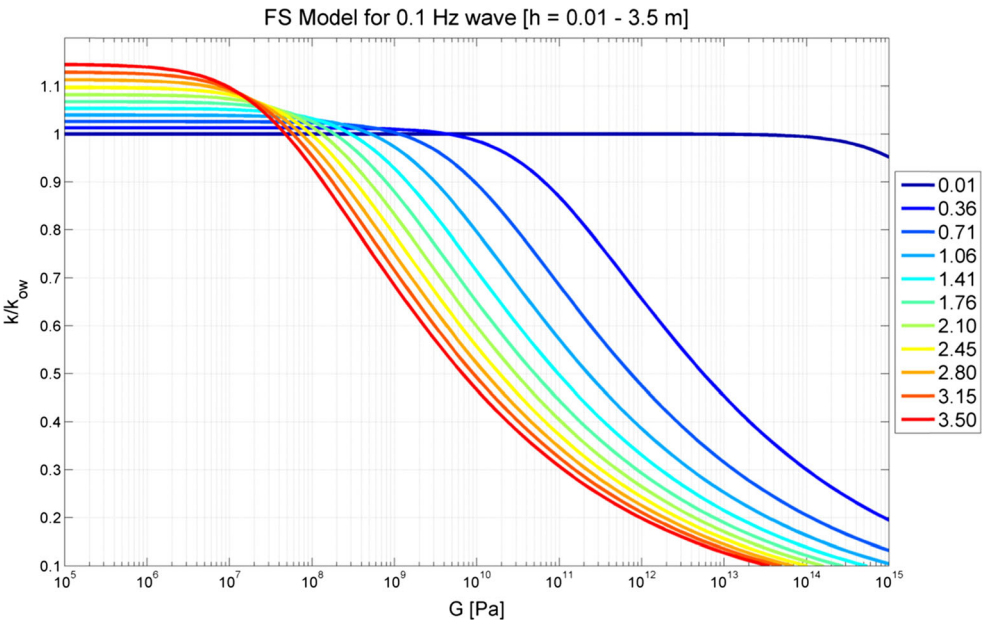

Fig. 3 Change is normalized wavenumber as a function of shear modulus, *G*, in the pure elastic model. Ice thickness shown in color as indicated in the legend

introduced into inviscid plate theory. First, the dispersion relation is formulated in terms of a complex wavenumber[4]:

$$k = k_0 + i\alpha \tag{17}$$

Assuming the real and imaginary parts are separable, solving for the real part of the dispersion relation gives the wavenumber and solving for the imaginary part gives the attenuation coefficient, α. Dissipation is introduced into Eq. (7) by including an additional imaginary term within the term proportional to k^4.

$$\frac{\omega^2}{g - M\omega^2 + Dk^4} = k \tag{18}$$

where D has a real part (B from Eq. (7)) and an imaginary part consisting of any number of specific complex formulations. We continue with the extended model of Fox and Squire (1994) (EFS) (Mosig et al. 2015). This is a Voigt model; it follows from analogy to a spring-dashpot and introduces dissipation (or friction) proportional to frequency. The dispersion relationship for EFS is as follows:

$$\frac{\omega^2}{g - M\omega^2 + \frac{G_v h^3}{6\rho}(1-\nu)k^4} = k \tag{19}$$

Here, G_v is complex Voigt shear modulus (Mosig et al. 2015) which is related to the elastic shear modulus, G, and the dissipation parameter[5] (related to the dashpot-constant), η:

$$G_v = G - i\omega\rho_{ice}\eta \tag{20}$$

so that Eq. (19) can be expanded to

$$\frac{\omega^2}{g - M\omega^2 + Bk^4 - i\omega\rho_{ice}\eta\frac{h^3}{6\rho}(1-\nu)k^4} = k \tag{21}$$

Figure 2 was produced by setting η to zero in Eq. (21), therefore reducing the EFS to the FS, and then varying the value of G. With all other parameters staying the same, and for the values of dissipation parameter tested, changing the dissipation parameter alone did not produce a significant change to the real part of the wavenumber and hence does not alter the wavelength (this is consistent with the dominant wave mode in Figs. 4 and 5 of Mosig et al. (2015)). Dissipation does, however, introduce attenuation.

Figure 4 shows the normalized dispersion relation on the left side and on the right the attenuation coefficient. From top to bottom, the ice thickness is 0.1, 0.5, 1.0, and 3.5 m, respectively. G is set to 2×10^9; the value used in Doble and Bidlot (2013) and the variation of η is shown with color. For the combination of parameters considered, wavenumber is not a function of dissipation parameter and all the dispersion curves lie on top of one another leaving only the last color plotted (dark red) visible. In contrast, attenuation curves progress monotonically with frequency and linearly with dissipation parameter.[6] The change in slope of attenuation for a specific value of the dissipation parameter can be seen to correspond with deviation from the open water dispersion relation. Given the same dissipation parameter, whether or not attenuation increases or decreases with a change in ice thickness depends on the frequency. Comparing the top and bottom plots on the right hand side, the lower frequency (<0.10 Hz) attenuation is drastically increased and the higher frequency (>0.30 Hz) attenuation is slightly decreased.

To explore this a bit further, values are set for elastic shear modulus, $G = 10^5$, and dissipation parameter, $\eta = 0.01$. The ice thickness is varied from 0 to 5 m. For reference, the solutions for the dispersion relation with ice thickness of 5 m for the mass loading model (ML) and purely elastic model (FS) are also shown.

The left side of Fig. 5 shows the dispersion relation calculated using the EFS model with color showing ice thickness. The solution for h = 5 m matches that of the FS exactly. The change in k is small for low frequencies and more pronounced for high frequencies. On the right side, attenuation is a function of frequency, with attenuation highest for the high frequencies. The change in slope for the attenuation corresponds with the dominant term in the dispersion relation transitioning of ML to flexural-gravity. Before the transition, the attenuation increased monotonically with thickness, the opposite is true after the transition, resulting in an unintuitive situation: high frequency (>0.50 Hz) waves in thinner ice encounter more attenuation. This behavior is similar to a common feature of models for water waves over seabed composed of a viscous mud layer, e.g., Dalrymple and Liu (1978): dissipation has a nonmonotonic dependence on mud layer thickness (see their Fig. 2), with thicker layers being less dissipative.

It should be kept in mind that the relationship being tested is based on the Euler-Bernoulli beam theory which is valid only for infinitesimal strains, and as the wave frequency increases, the reflection approaches 100% (Fox and Squire 1994).

[4] In the literature, the imaginary part of the complex wavenumber is also denoted as k_i or q

[5] In Mosig et al. [2015], this is called viscosity parameter, but here, we use dissipation to avoid confusion with viscous-layer model introduced in the following section. The symbol η is not to be confused with sea surface elevation.

[6] A reviewer pointed out that an asymptotic expansion in the dissipation parameter should be possible.

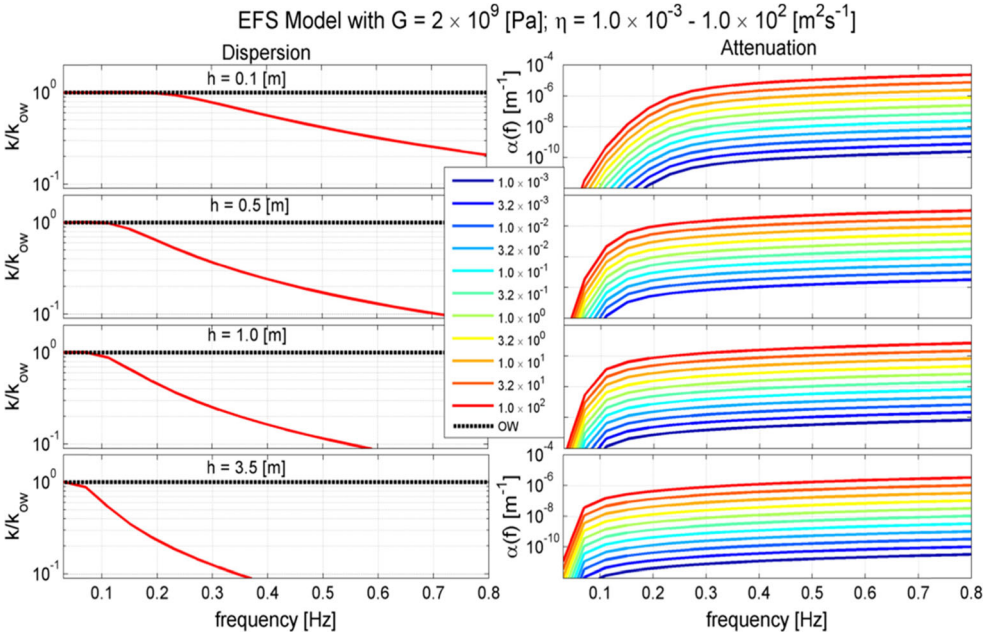

Fig. 4 *Left side*: normalized wave number relation. *Right side*: corresponding attenuation coefficient. From *top to bottom* the ice thickness is 0.1, 0.5, 1.0, and 3.5 m. The *colors* indicate the dissipation parameter ranging over five decades. The dispersion relation does not change as a function of dissipation parameter, therefore all lines are over plotted and the only visible line is *dark red* (last one plotted) and the *black dotted line* is the open water relation

2.3 Viscous-layer models

Instead of an elastic plate, the problem can be formulated in a two-layer model. Ice would be represented by a layer of viscous fluid on top of a slightly viscous or inviscid layer by keeping viscosity in the Navier-Stokes equation (Weber 1987; Keller 1998; De Carolis and Desiderio 2002). In these models, the ice does not have flexural properties, and the two free parameters are ice thickness and an effective viscosity parameter. Please see the original references for the closed forms of the dispersion relations which are omitted here.

The model of Wang and Shen (2010a) extended the model of Keller (1998) to incorporate elasticity. Thus, Keller's viscous model can be recovered by setting the effective shear modulus to zero in the model of Wang and Shen (2010a). Figure 6 is produced in this way, using the model of Wang and Shen (2010a) as implemented in WAVEWATCH III® (Tolman and the WAVEWATCH III® Development Group 2014), and varying the viscosity parameter, η, over nine decades for several thicknesses.

In the viscous-layer formulation, in contrast to dissipation in the EFS model, effective viscosity results in a deviation from the open water wavenumber. For the low frequencies, the wavenumber is slightly increased compared to ML, through the mid-range frequencies k approaches the ML relation. The different behaviors in the high frequencies can be described in terms of a Reynolds number, $R_n = \sqrt{gh^3}/\eta$ (Keller 1998). For very large Reynolds numbers, there is no

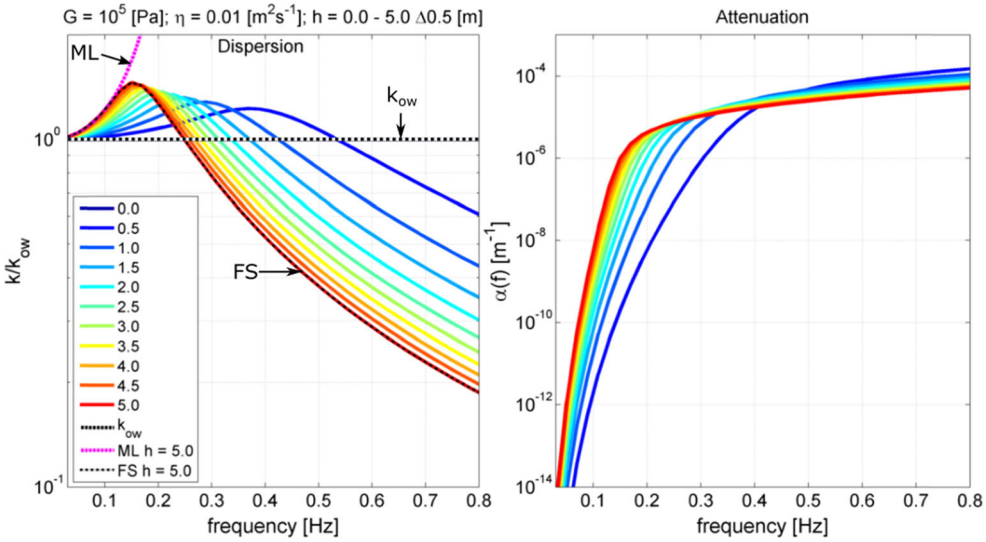

Fig. 5 *Left side*: normalized wave number as a function of frequency. *Right side*: the corresponding attenuation rate. The *color* indicates ice thickness, h. Shear modulus is set to the value 10^5 and dissipation parameter to the value 0.01. The mass loading model (ML) and purely elastic model (FS) are shown for $h = 5.0$ m with the *magenta dotted line* and *black dashed line*, respectively

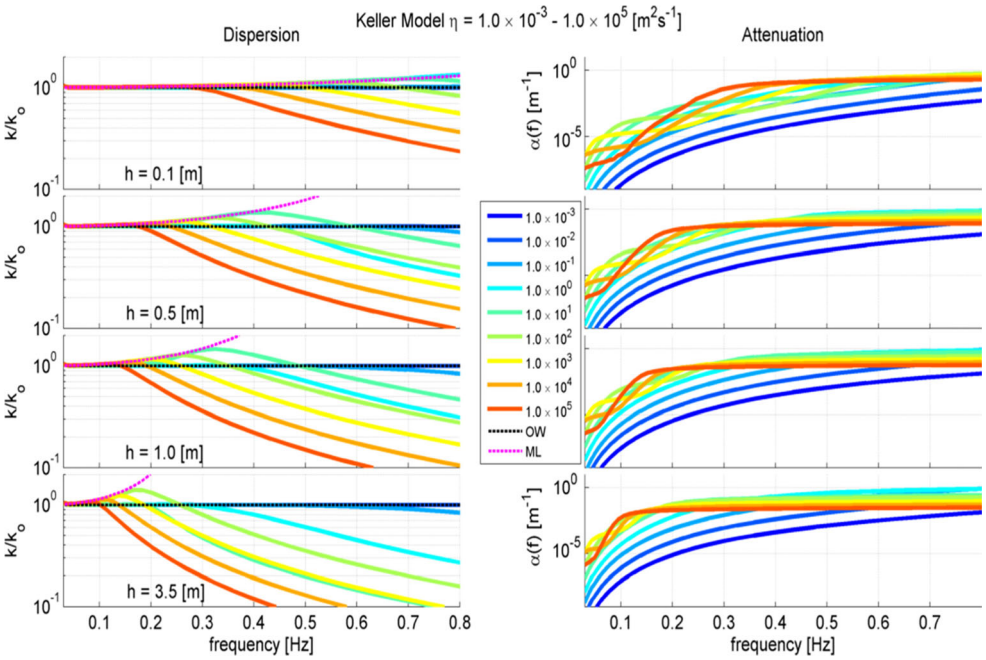

Fig. 6 Results from evaluating the viscous-layer model of Keller (1998). *Left side*: normalized wavenumber as a function of frequency. *Right side*: the corresponding attenuation. From *top to bottom* the ice thickness is 0.1, 0.5, 1.0, and 3.5 m. The *colors* indicate the viscosity of the viscous-layer ranging over nine decades

significant change in wavenumber, and the attenuation has a constant slope in frequency. With small Reynolds numbers, the wavenumber behavior is similar to the FS model in that the wavenumber follows the ML model as an upper bound, and at a particular frequency, the wavenumber precipitates. At intermediate Reynolds numbers, the wavenumber tends to stay closer to the open water relation before rapidly decreasing. The attenuation, although monotonically increasing with frequency, changes the slope in sync with changes in slope of normalized wavenumber. For both the low and the high frequencies, increasing η increases attenuation up to a point, then it begins to decrease again. For a very high η, there is a leveling out of attenuation in the high frequencies at the point where wavenumber dips below the open water value.

Newyear and Martin (1999) gave $\eta = (3.0 \pm 0.25) \times 10^{-2}$ m^2 s^{-1} as a fit to their laboratory data. At this effective viscosity, there is a little or no change in wavenumber except for at the highest frequency and largest thickness tested (bottom panels of Fig. 6) where a decrease is evident.

For combinations of high frequencies and large thickness, a small change in viscosity parameter results in a large difference in wavenumber near $R_n = 1$.

This behavior is demonstrated in Fig. 7. For the wave frequency 0.39 Hz, there is a discontinuity in the normalized wavenumber near $R_n = 1$ for the thickness of 3.50 and 1.00 m. For the other thickness-frequency combinations, there is a smooth transition across layer viscosity. This may be related to the method of choosing a wave mode (or root), in this

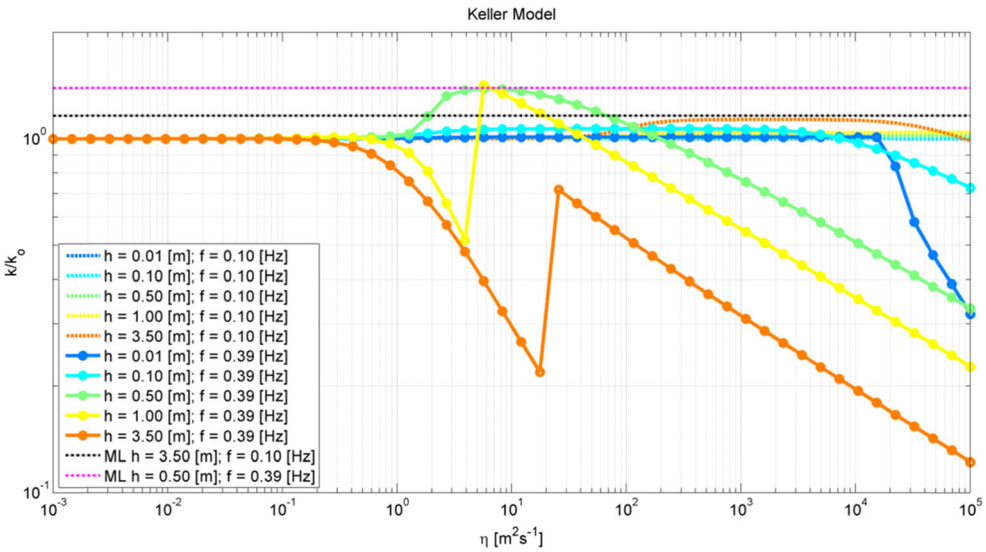

Fig. 7 Keller model as a function of layer viscosity over eight decades for combinations of frequency and thickness. The *dashed lines* indicate a frequency of 0.10 Hz while the *solid line* corresponds to 0.39 Hz. The *cool to warm colors* indicate thicknesses of 0.01, 0.10, 0.50, 1.00, and 3.50 m, respectively. Two results for the ML are shown for reference with *magenta* and *black dashed lines*. The curves for $f = 0.10$ Hz stick close to $k/k_{ow} = 1$ and are mostly hidden behind the small thickness curves for $f = 0.39$ Hz

case, the least attenuating wave mode was chosen (Zhao et al. 2015). The ML model is shown to bind an increase in wavenumber. The effect of viscosity in the Keller model is to decrease the wavenumber.

2.4 Note on viscoelastic models

Models which combine dissipation and elasticity are collectively known as viscoelastic dispersion models (Robinson and Palmer 1990; Wang and Shen 2010a; Mosig et al. 2015). This is achieved by introducing dissipation into plate theory, or, in the case of Wang and Shen (2010a), by generalizing the viscous-layer theory of Keller (1998) to include viscosity. The models Wang and Shen (2010a) and Robinson and Palmer (1990) were not explored here; for a detailed comparison, see Mosig et al. (2015).

3 Refraction and shoaling

The original motivation for this study stemmed from interest in ice-fracture events (Asplin et al. 2012; Kohout et al. 2014; Collins et al. 2015; Kohout et al. 2015) and whether or not the wave height changes upon entering ice. An important consequence of an altered dispersion relationship, in terms of the stress felt by the ice, is the change in wave height. In direct analogy for refraction and shoaling in shallow water (or in horizontally shearing currents), it can be shown that a wave propagating across a material gradient will change the group speed and correspondingly change the direction and amplitude. These changes can be derived with Snell's law, most commonly encountered in the context of geometric optics, applied to ocean waves (e.g., Dean and Dalrymple (1991)).

If the wavelength shortens, then the waves will turn towards the vector normal to the ice edge. This is similar to a situation of waves entering an opposing current approaching the shore at an angle: waves always turn to approach shore-normal. If the wavelength increases, the waves will turn away from the vector normal to the ice edge, similar to waves approaching a following current at an angle.

To get Snell's law in ice, consider monochromatic waves approaching an ice field with slowly varying properties (e.g., Kirby (1992)). Wave crests approach the ice field at some angle, θ, off-normal to the ice edge and let φ be the corresponding angle between the wave crests and the ice edge. According to Snell's law, waves traveling in material 1 and 2 must obey the following relationship:

$$\frac{\sin(\varphi_1)}{\sin(\varphi_2)} = \frac{C_1}{C_2} = \frac{\lambda_1}{\lambda_2} \tag{22}$$

where C is the phase speed and λ the wavelength. The phase and group speed in open, deep water (ow) follows from the linear dispersion relation:

$$C \equiv \frac{\omega}{k}, C_g \equiv \frac{\partial \omega}{\partial k} \tag{23}$$

$$C_{ow} = \sqrt{\frac{g}{k}}, C_{g,ow} = \frac{1}{2}\sqrt{\frac{g}{k}} \tag{24}$$

As a wave crosses into ice covered regions, Snell's law determines the refraction angle:

$$\frac{\sin(\varphi_{ice})}{\sin(\varphi_{ow})} = \frac{\sin(\theta_{ice})}{\sin(\theta_{ow})} = \frac{C_{ice}}{C_{ow}} = \frac{k_{ow}}{k_{ice}} = \frac{\lambda_{ice}}{\lambda_{ow}} \tag{25}$$

$$\theta_{ice} = \arcsin\left(\frac{k_{ow}}{k_{ice}}\sin(\theta_{ow})\right) \tag{26}$$

The change in wave height is derived by conserving the mean energy per unit area, which can be determined from the spectrum by linear theory (Kinsman 1965). The wave energy per unit crest length is the integral of spectral density scaled by gravity and the density of water:

$$E = 2\rho g \int F(f) df = \frac{1}{8}\rho g H_{m_0}^2 \tag{27}$$

Wave energy propagates at the group speed which defines the energy flux, P_E

$$P_E \equiv E C_g \tag{28}$$

assuming a constant energy flux along a section of crest width, s,

$$P_{E,ice} s_{ice} = P_{E,ow} s_{ow} \tag{29}$$

$$\frac{\rho g}{8} H_{m_0,ice}^2 C_{g,ice} s_{ice} = \frac{\rho g}{8} H_{m_0,ow}^2 C_{g,ow} s_{ow} \tag{30}$$

solving for wave height in ice

$$H_{m_0,ice} = H_{m_0,ow}\left(\frac{C_{g,ow}}{C_{g,ice}}\right)^{\frac{1}{2}}\left(\frac{s_{ow}}{s_{ice}}\right)^{\frac{1}{2}} = H_{m_0,ow} DK \tag{31}$$

where K, known as the refraction coefficient, is the square root of the ratio of the crest lengths from Snell's law which can be written in terms of the refraction angles

$$K = \left(\frac{\cos\varphi_{ow}}{\cos\varphi_{ice}}\right)^{\frac{1}{2}} \tag{32}$$

and D, known as the shoaling coefficient, is the square root of ratio of the group velocities, with $C_{g,ice}$ chosen appropriately for the ice conditions

$$D = \left(\frac{\frac{1}{2}\sqrt{\frac{g}{k_{ow}}}}{C_{g,ice}} \right)^{\frac{1}{2}} \tag{33}$$

The implication is this: if the group velocity slows in ice, then wave heights will increase and if the group velocity increases in ice, then wave heights will decrease. In terms of the wave effects on ice, this will change the stress felt by the ice since the wave-induced stress is a function of the wave slope. To reiterate, a decreasing group velocity results in an increasing wave height and because of the increased wave height, ice-shoaled waves will result in a greater (than expected from open water dispersion) stress on the ice leading to fracturing which might not otherwise occur.

In addition, there are unexplored aspects of phase-dependent wave dynamics in ice which may appear due to change of dispersion through (1) altered interaction space for resonant triad and quadruplet interactions and (2) increased or decreased steepness of the waves. The steepness may increase the likelihood that the waves will be unstable possibly leading to modulational perturbations (nonresonant, quadruplet interactions) or wave breaking, this has been shown to be important for waves shoaling on an opposing current (Toffoli et al. 2015).

Conversely, if the wavelength increases and/or the wave height decreases, then the stress felt by the ice will be less relative to that expected from open water conditions. In a coupled wave-ice model (e.g., Williams et al. 2013a, 2013b; Horvat and Tziperman 2015), it will be imperative to accurately account for the wave-induced stresses on ice.

The shoaling and refraction effects are expected to be the most important in the vicinity of the ice edge as attenuation becomes important over long distances. Effects will be less dramatic along a diffuse wave-ice interface as in the winter ice expansion of the Arctic MIZ.

4 Measurement of wave dispersion in ice

A number of mathematical models for dispersion of surface waves in ice have been investigated, and although some of the closed forms of dispersion relations are simple to write, the solutions produced can be complex. To verify the solutions produced by a dispersion model, comparison to measurements needs to be performed, but this has proved challenging in practice. The difficulty is that estimation of the dispersion requires spatiotemporal information, i.e., colocated measurements of wave period and wavelength. In the following subsections, visual, remote, in situ, and laboratory observations of dispersion are summarized and tabulated (Table 1).

4.1 Visual

The account of the chief scientist of the R/V Polarstern, E. Augstein, was reported by Liu and Mollo-Christensen (1988) and further expanded on by Broström and Christensen (2008). Approximately, 560 km from the ice edge, waves of 1 m height, and 18-s period broke up the ice and caused a significant rafting. The wavelength before the ice broke was reported to be much shorter than the wavelength in broken ice which motivated the formulation of the dispersion relation with compressive stress (Liu and Mollo-Christensen 1988).

4.2 Remote sensing: SAR

A number of studies have attempted to use airborne or satellite synthetic aperture radar (SAR) imagery to observe the change in wave directional-spectra upon entering ice (Wadhams and Holt 1991; Liu et al. 1991; Shuchman et al. 1994; Wadhams et al. 2002; De Carolis 2003; Wadhams et al. 2004). Wadhams and Holt (1991) found that the wavelength decreased in frazil and pancake ice in the Chukchi Sea in October. They inverted the mass loading model to estimate the ice thickness, which was later found to be overestimated (Wadhams et al. 2004; Squire 2007). Liu et al. (1991) combined open water buoy measurements with SAR imagery over compact ice cover, with an average thickness of 1.5 m and brash ice connecting floes, to achieve two independent measurements of dispersion. For the two cases, they found (1) the peak wavelength increased from ~150 to ~225 m and (2) the peak wavelength shortened from ~395 to ~345 m. Comparing to a viscoelastic model, they found a reasonable agreement for case (1) using a h = 2 m and depth = 150 m and for case (2) h = 1 m and depth = 75 m. Shuchman et al. (1994) studied two different cases (March 1987 and March 1989) in pack ice and a pancake ice tongue with opposing results: lengthening and shortening, respectively. Wadhams et al. (2002) analyzed five datasets of frazil-pancake ice, with ground validation in some cases, and found a consistent decrease in wavelength (see Wadhams et al. (2002) for an explanation of the various locations and seasons). De Carolis (2003) found shortened waves in March in pancake ice from the Odden Tongue. Wadhams et al. (2004) observed decreased wavelengths in frazil and pancake ice during April in the Antarctic, and in situ measurements verified the ice parameters inverted from the viscous-layer model of Keller (1998).

4.3 In situ

Strainmeters, tiltmeters, and seismometers have been used to determine the elastic properties of ice sheets, typically by

Table 1 Change of wavelength in the field

Reference	Measurement	Timing	Location	Ice type	−Shortened, +lengthened	f (Hz)
Squire and Allan 1977	Strainmeter	Jan–March	Newfoundland	Sheet of fast ice	−	0.25–0.33
Liu and Mollo-Christensen 1988	Visual report & ships radar	Winter	Weddell sea	Pack ice	−	0.056
Wadhams and Holt 1991	SAR	October	Chukchi sea	Frazil and pancake	−	~0.09
Liu et al. 1991 (case 1)	SAR and buoy	March	Atlantic East of Newfoundland	O(10 m) floes in brash	+	0.10
Liu et al. 1991(case 2)	SAR and buoy	March	Atlantic East of Newfoundland	O(10 m) floes in brash	−	0.06
Shuchman et al. 1994 (case 1)	SAR	Spring	Fram strait	Pancakes to pack ice	+	?
Shuchman et al. 1994 (case 2)	SAR	Spring	Odden tongue	Grease and pancake	+	?
Fox and Haskell 2001	Floe mounted accelerometers	June	Antarctic	Densely packed pancakes	+/−	0.05–0.10/0.10–0.16
Wadhams et al. 2002	SAR and buoy	Variable	Variable	Frazil and pancake	−	Variable
De Carolis 2003	SAR	March	Odden tongue	Frazil and pancake	−	?
Wadhams et al. 2004	SAR	April	Antarctic	Frazil and pancake	−	?
Marsan et al. 2012	Seismometers	Spring	North pole	Deep pack ice	+	0.05–0.20
Sutherland and Rabault 2016	Accelerometers	March	Templefjorden, Savlbard	Sheet of fast ice	+/0	0.10–0.20

assuming an elastic (flexural-gravity) dispersion relation (e.g., Ewing and Crary (1934), Tabata (1958), and Stein et al. (1998)). Only a few verify the dispersion relationship itself. Squire and Allan (1977) calculated the coherence between three strainmeters at short distances O (10 m) on a 0.5-m thick sheet of fast ice in Newfoundland. Only in the range of 0.25–0.33 Hz did wavelength significantly vary from the open water relation, matching the longer wavelength prediction of an elastic model for 0.5 m ice. Marsan et al. (2012) used the correlation between seismometers deployed near the North Pole on Arctic pack ice to show the group velocity matched that of flexural-gravity waves (see their Fig. 7).

In the Antarctic MIZ, Fox and Haskell (2001) mounted two accelerometers to two elliptic pancake ice floes. The floes were estimated to be 0.3 and 0.6 m thick, but were not otherwise characterized. By choosing two closely located positions, they were able to estimate the propagation speeds of waves (and hence indirectly the wavelength) in ice by measuring the frequency spectrum. Fig. 6 shows that the fitted empirical wavelength is slightly longer for frequencies within the 0.05–0.10-Hz band and then significantly shorter for frequencies from the 0.10–0.16-Hz band and a fitted dispersion relation gave $k \propto \omega^{2.41}$. For comparison, the open water relation gives $k \propto \omega^2$. It is difficult to explain the lengthening of the low frequencies, but the decrease in wavelength of high frequency waves is essentially consistent with mass loading.[7]

[7] However, Fox and Haskell [2001] did not make this connection: "While the added-mass and ice-sheet models predict dispersion equations with power laws less than 2, we found that the measured dispersion equation has a power law with exponent greater than 2." Referring to either the statement or the result, Squire said it was "perplexing" in his 2007 review paper.

Sutherland and Rabault (2016) correlated the signals between nearby accelerometers (<1 peak wavelength) deployed in fast ice in a fjord in Svalbard (Norway) in March. They found that the dispersion relation matched that for flexural-gravity waves until the ice sheet became significantly cracked at which point the dispersion more closely matched the open water relation.

4.4 Laboratory

Although there have been a number of experiments in the laboratory, generalization of results from laboratories is questionable given the large disparity in scales, for example lab experiments are limited to very high frequency waves (>0.40 Hz). Nevertheless, a few of the more salient studies are summarized here. Newyear and Martin (1999), in experiments with grease ice, found that wavelengths increase according to the viscous model of Keller (1998). Sakai and Hanai (2002), in an experiment with synthetic ice, found that the dispersion relationship (between 0.6 and 1.7 Hz) varied between a flexural model and a mass-loading model as a function of floe length scale. It stands to a reason that this transition must have been dependent on the relative scales of the wavelengths and floe sizes so that at any time the measured dispersion relation was not dominated by either the mass loading or the flexural-gravity terms in the theoretical dispersion relation. The higher frequencies showed the greatest ranges of celerity as a function of ice thickness. Wang and Shen (2010b) extended the experiments in Newyear and Martin (1999) to lower frequencies and pancakes in grease ice and found the model of Keller (1998) no longer sufficiently described the dispersion

and attenuation for the case of pancake ice. Zhao et al. (2015) inverted the effective viscoelastic parameters of the Wang and Shen (2010a) model from three different ice types.

5 Discussion

5.1 Models

5.1.1 Implementation in spectral wave models

Third generation, spectral wave models are the workhorses responsible for operational prediction of sea state, and these models solve for evolution of wave action, N, in the radiative transfer equation:

$$\frac{DN}{Dt} = \sum \frac{S}{\sigma} \tag{34}$$

The left side is the propagation term and the right side is the source and sink terms. Consider spectral density, $F = N\sigma$, which attenuates as a function of distance, x:

$$F(f,x) = F(f,0)\exp(ikx) \tag{35}$$

substituting in the complex wavenumber

$$\begin{aligned} F(f,x) &= F(f,0)\exp(ix(k_0 + i\alpha)) \\ &= F(f,0)\exp(-\alpha x)\exp(ik_0 x) \end{aligned} \tag{36}$$

On the right hand side, $F(f,0)$ is the spectral density, the first exponential is the attenuating mode, and the second exponential is the oscillatory mode. Given the group velocity, C_g, the attenuation coefficient may be written in terms of the space or time domain. Writing the attenuation rate as a function of distance serves as the implementation of an ice "source term", S_{ice}, on the right hand side of Eq. (34) (Rogers and Zieger 2014):

$$\frac{S_{ice}}{F} = -2C_g\alpha \tag{37}$$

Attenuation, α, comes from the imaginary part of the dispersion relation, and group velocity, C_g, is derived from the real part. The change in group velocity informs the propagation on the left hand side, and results in shoaling and refraction.

5.1.2 Generalized plate theory

In Fig. 2 the normalized wavenumber goes below the scale on the y-axis for combinations of high frequencies and thick ice and similarly in Fig. 3 for combinations of thick ice and high G. Indeed, in the limit of high frequencies, large thickness, and high G, the wavenumber approaches infinity, and the wave velocity becomes unbounded. In response to this issue, Mindlin (1951) provided a more general plate theory which included the effects of rotary inertia and shear. The rotary inertia and shear terms effectively bound the problem and acted as correction terms. For this reason, it may be of interest to apply Mindlin's plate theory in operational models. For more details, see Mindlin (1951), in particular Fig. 1, and Meylan and Squire (1995).

5.1.3 Choosing a root

Solving the dispersion relation, particularly for the more complicated viscoelastic models, gives rich solutions with a number of choices for the root. In the EFS model, for very high frequencies, >1.0 Hz, errors with the solver (not shown) arose. In a plot similar to Fig. 5, following a dispersion relation for constant thickness from low to high frequencies, wavelength appeared to suddenly increase by many orders of magnitude (correspondingly, attenuation appeared step-wise). It was discovered that this was an artifact of the numerical solver giving the wrong root (e.g., see Mosig et al. (2015)) because the parameters involved were probably outside the validity of the model (personal communication with V. Squire, 2015). According to Mosig et al. (2015), who compared three viscoelastic models, other dispersion models are also susceptible to these sorts of errors. As corroboration, artifacts of the root choosing system are apparent Fig. 7. Devising a system for choosing roots of the complex dispersion relation (e.g., Zhao et al. (2015)) is an ongoing challenge for those who seek routine implementation of these models.

5.2 Measurement deficiencies

The measurements of the dispersion relationship in ice are much fewer than those of attenuation, and hence, empirically, the dispersion relationship is even less well understood than attenuation. There are a number of deficiencies in the existing observations. The ranges of frequencies covered by the observations have been limited to that of the peak or a small band, when ideally the whole range of wind-wave frequencies needs to be characterized for each ice type.

Analyzing SAR imagery for waves is not a trivial endeavor in itself, in particular the studies of Wadhams and Holt (1991), Liu et al. (1991), Shuchman et al. (1994) may be compromised by simplified analysis (see discussion in Wadhams et al. (2002)). To properly calculate a wavenumber spectrum, a modulation transfer function must be applied, the details of which are still a matter of intense investigation (Zhang et al. 2010). In addition, the imaging mechanisms may change in ice (Ardhuin et al. 2015). In many cases, there was no in situ verification of the open water SAR analysis, and even when there was, often it was the change in peak wavelength that was reported. For any estimated spectrum, the resolution of the

low frequencies is poor; the spatial resolution of the SAR itself may also be quite low, so that a shift of even one frequency bin may equate a large change in wavelength. This may, in part, explain the overestimation of ice thickness from the ML model (P. Wadhams, personal communication, 2016). Reporting just the change in peak wavelength is additionally complicated by the fact that attenuation usually preferentially damps high frequency waves, leading to a shift in the peak to lower frequencies unrelated to dispersion.[8] If swell has already traveled a long distance from the generation area, an increase of the wavelength in the wave direction may be expected from normal velocity dispersion (Snodgrass et al. 1966), but there will be no coincident change in direction as is expected with wave-ice interaction.

One major caveat applies to all the observations reviewed: there were no accompanying current measurements. In deep water, it is widely known that wave-current interaction causes a change in dispersion and the associated shoaling and refraction. Implicit to all of the above studies is the observation of the intrinsic frequency, or in other words, observing the wave frequency in the reference frame of the mean currents. The dispersion observed in a Eulerian reference frame in the presence of currents has an extra term:

$$\omega_E = \sqrt{gk} + \boldsymbol{k}\cdot\boldsymbol{U} \tag{38}$$

where $\boldsymbol{k}$ and $\boldsymbol{U}$ are the wavenumber vector and current vector, respectively. Opposing currents decrease frequencies while following currents increase frequencies. Future observations will need to account for currents.

For completeness, wave amplitude also affects dispersion. According to Stokes theory, which uses an expansion on steepness as a small parameter, the third order dispersion relation has a dependence on wave amplitude, A (e.g., Whitham (2011)):

$$\frac{\omega^2}{g\left(1 + k^2A^2 + O\left((ka)^4\right)\right)} = k \tag{39}$$

Meaning that wavelength increases for steep waves, though the effect is small for ocean waves of typical steepness. Also, the skewness of waves introduces bound harmonics, these are waves with frequencies at integer multiples of the fundamental frequency but traveling at the same speed as the fundamental ones. These bound waves have been observed to be important at very high frequencies, $f > 3f_p$ (Leckler et al. 2015). If dealing with measurements of very steep or very high frequency waves, one should be cognizant of these effects.

[8] For the cases of shortening, this implies even a stronger change in dispersion than measured, and for the cases of lengthening this implies a lesser change in dispersion (or none at all).

5.3 A picture of the status quo

Due to the difficulty of conducting thorough observations and the variable nature of ice, the best that can be offered is a qualitative outlook, far from comprehensive, drawn from the overlap between theory and measurements. For the MIZ, over the course of a year starting with the autumn refreeze, ice crystals (frazil ice) form, and conglomerate on the surface. With enough frazil, small wavelets are damped, and the surface appears slick (so-called grease ice). In the absence of waves, sheets of nilas form. In the presence of waves, grease ice is shaped into almost spherical conglomerations which grow into pancake ice (Wadhams 2000). These pancakes increase in concentration as one travels from open water into the central pack ice. This central ice pack is characterized by “cemented” first-year pancakes and multiyear floes. As waves enter the MIZ from open water, the floes may be sparse and one might expect a decrease in wavelength by simple mass loading. In the case of grease ice, a viscous-layer model may be appropriate. Going deeper into the MIZ, as the concentration of floes increases so does the influence of other factors such as effective viscosity or elastic properties of the brash or frazil ice layer in between the pancakes. Eventually the floes will consolidate, forming a solid layer with strong elastic properties which support lengthened flexural-gravity waves if the incoming waves do not attenuate entirely before reaching this point.

The low frequency waves deviate less from the linear dispersion relationship and correspondingly attenuate less. It may be possible for extremely low frequency waves (~25 s) to propagate great distances, if not all the way through, the central Arctic ice pack (Wadhams and Doble 2009; Ardhuin et al. 2016a). Very high frequency waves deviate the most from the linear dispersion relationship, but they are also more quickly attenuated such that very high frequency waves do not exist very far into the MIZ.

Once the ice is more or less solid, the bending of the ice, induced by incoming waves, may exceed the breaking stress directly or by fatigue, and the ice breaks apart into floes which no longer support flexural-gravity waves. The flexural strength of ice weakens as the temperatures rise and ice experiences the summer melt. Eventually the MIZ is extended and pushed northward as more ice is broken by incoming waves.

These broad, qualitative statements more or less sum up the state of knowledge regarding wave dispersion processes in the Arctic. This descriptive understanding of wave-ice interaction is well short of what is needed to improve wave forecasting in ice. Certainly, more sophisticated measurements with an increased sensitivity over larger frequency ranges are necessary. A handful of modern techniques may be suitable for this purpose.

5.4 Future prospects

SAR imaging will continue to offer a window in the wave dynamics in sea ice, but clearly, there is still much more work to be done to advance the current methods. A promising new avenue for SAR analysis is the work of Ardhuin et al. (2015) and Ardhuin et al. (2016b). Without a temporal component, SAR data will always be inherently limited. Ideally, a measurement of dispersion would have both spatial and temporal components.

A previously overlooked possibility is the complementary signals from heave-pitch-roll (e.g., common directional wave buoys) whose cross-correlation allows the estimation of the low-order directional moments (Longuet-Higgins et al. 1963; Collins et al. 2014). Wavenumber as a function of frequency can be estimated from the autocorrelation of these the same signals (see discussion of Longuet-Higgins et al. 1963; Appendix A of Kuik et al. 1988). Denoting C_{xx} and C_{yy}, the autocorrelations of the slope signals in the horizontal plane, C_{zz} the autocorrelation of the sea surface elevation, and k_e the estimated wavenumber:

$$C_{xx} + C_{yy} = k_e^2 C_{zz} \tag{40}$$

so that

$$k_e = \sqrt{\frac{C_{xx} + C_{yy}}{C_{zz}}} \tag{41}$$

k_e is commonly used as an alternative to assuming the open water linear relation in formulating the lower order directional moments (Long 1980), but it has not typically been evaluated as a measurement of the dispersion relation. This is because the motion of a buoy may not exactly follow the ocean surface. In this context, the formula has been used as a quality control measure by comparing against the expected open water relation in a so-called check ratio (Tucker 1989, Tucker and Pitt 2001). A similar check relation for displacement buoys has been used to flag the influence of currents, mooring forces, and biofouling on buoy response (Thomson et al. 2015).

If there is uncertainty about the response of a buoy, then tracking the change in k_e across an array of similar buoys would at least provide whether waves were shortening or lengthening. To avoid the issue of buoy response, one could combine a time series with spatial measurement such as colocated, coincident time series, and spatial measurement, e.g., a laser rangefinder and a scanning LIDAR.

The ideal systems for measuring wave dispersion are natively spatiotemporal. One such system is stereo-video (e.g. Campbell et al. (2014)) and another is ship-borne, X-band marine radar (MR) (Young et al. 1985; Borge et al. 1999; Lund et al. 2014; Lund et al. 2015). Both of these systems directly measure wave dispersion (Krogstad and Trulsen 2010), and in principle, the contribution from ice can be uniquely determined.

A sequence of images is 3-D Fourier transformed into wavenumber-frequency spectra. In wavenumber-frequency space, the energy is iteratively fitted to a current-free dispersion shell; the occurrence of a deviation of energy from the dispersion shell indicates the presence of currents. The presence of a current has a directionally dependent signature, shifting energy according to the relative angle between the wave propagation direction and the current direction. Since a dispersion change due to ice has no directional dependence, it should be possible to use this method to uniquely determine the ice induced deviation from an open water dispersion.

There are drawbacks, even with these systems. Marine radars have limited frequency resolutions, typically up to 0.30 Hz, and stereo-video systems sample a limited spatial extent of the sea surface which sets a lower limit for k.

Even with a perfect system, a comprehensive measurement is difficult because of the inherent tradeoffs. At each frequency band are at least two tradeoffs, (1) between the expected deviation from open water dispersion (higher frequencies deviate more) and the strength of the wave signal (higher frequencies suffer higher attenuation) and (2) between the influence and presence of ice (increasing effect on dispersion). As short waves are attenuated, the peak waves become lower in frequency and deviate less from open water dispersion. To say it in another way: the short waves which best demonstrate a change in dispersion are also expected to have a weak or nonexistent signal due to attenuation. Where the short waves exist, near the open water edge of the MIZ, there is less ice and hence waves are less ice affected.

Measurements of dispersion in ice are a manifestation of the individual mechanisms of wave-ice interaction and thus, like attenuation, the effect of these mechanisms are difficult, if not impossible, to separate. Whereas mechanisms responsible for attenuation in the direction of wave propagation (reflection, scattering, turbulence, eddy viscosity, etc.) always lead to a decrease in energy, the outcomes of the individual dispersion mechanisms are mixed (i.e., there may be a balance of mechanisms which increase and decrease wavelength). In other words, it is possible for dispersion to be governed by dynamics that are altered from open water, yet there is no change in wavelength for a range of frequencies (i.e., a range where $k/k_{ow} \cong 1$). Therefore, a good understanding of the ice conditions must accompany the wave measurements.

5.5 Ice and unresolved processes

Much of the uncertainty about wave-ice interaction lies not with our understanding of waves, but with our limited understanding of sea ice (see Timco and Weeks (2010)). How waves behave in ice depends on the nature of the sea ice encountered. Before applying a particular dispersion model, large scale

Fig. 8 *Top*: still shot from a video of 4 m waves propagating through pancake ice within a frazil ice slurry in the Arctic MIZ taken by author WER during the field observations for ONR "Sea State" project in fall of 2015 in the Beaufort Sea. *Bottom*: still shot taken from a video of 1–2 m waves propagating in small floes with thick slush in between floes taken by author COC from R/V Lance (the bow in the left side of the image) in May of 2016 in the Barents Sea

characteristics should be known in approximation: is the ice more like a uniform, thin sheet, or is it a conglomeration of floes? Are these floes densely packed or spaced out? Are characteristic floe sizes large or small compared to the characteristic wavelength? Is there a layer of slurry-like frazil ice? The assumption of ice as a continuum needs to be evaluated as it may be a gross oversimplification in some cases.

When designing a forecast or hindcast with a spectral wave model, the character of the ice should lead to the appropriate dispersion model and inform the values of the model parameters. Unfortunately, wave measurements are not typically accompanied by mechanical measurements of ice. For large scale wave prediction, input from remote sensing will be important. However, there is not yet a detailed understanding of the relationships (if any exist) between (1) the available remote sensing products (i.e., concentration, thickness, age) (2) the ice type (e.g., pancake, frazil, grease), and (3) the mechanical properties of each ice type.

There are scenarios in which ice defies simple characterization and the application of the mechanical models discussed in this investigation is no longer sufficient. This happens with mixed ice types or when unresolved processes become important. The viscoelastic model of Wang and Shen (2010a) circumvents these scenarios by using an effective elasticity and an effective shear modulus, i.e., model parameters that would not result from measuring the mechanical properties of the ice. In fact, the practice has been to first measure dispersion and attenuation, then invert the model to give these effective parameters (Wang and Shen 2010b; Zhao et al. 2015). On the one hand, it is backwards to invert ice parameters from the waves instead of determining them from the ice these parameters ostensibly represent, but on the other hand, it is a convenient solution to an otherwise obscure problem.

The top part of Fig. 8 shows large waves in relatively small, uniform pancake ice which are forming in a frazil matrix. The floes converge and diverge with each wave cycle, bumping into each other. The mechanical properties of this ice type are obviously not the same as the mechanical properties of the ice in the lower part of the figure. In the lower photo, there are

waves propagating in floes, all smaller than the characteristic wavelength but of various shapes and forms. This ice type occurs as waves break up the consolidated pack ice during the summer ice retreat. The remote sensing products which currently inform wave models would give identical concentrations and thicknesses, but clearly there are many more nuanced interactions that cannot be determined from concentration and thickness alone. These interactions are not included in the simple mechanical models of ice. In both cases, all of the unresolved processes, including floe on floe interactions, are wrapped up into effective viscoelastic properties that can only be inferred by measuring the dispersion and attenuation.

In terms of operational wave models and coupled wave-ice models, an additional complication time and space scales which (1) are not adequately sampled by any existing operational method and (2) may be in violation of slowly varying assumption necessary for the spectral representation of wave evolution.

6 Concluding Remarks

Dispersion is one mechanism by which wave-ice interaction is implemented in Wavewatch III (Rogers and Zieger 2014), and understanding wave dispersion in ice, is therefore crucial for accurate prediction of wave characteristics and the corresponding ice conditions in the polar seas. Wave prediction currently relies on a small number of mechanical models for wave dispersion in ice, for which there are very few measurements for comparison. There has yet to be significant evidence in favor of one dispersion model over another, and different models will be more or less appropriate for different ice types. On the other side of the coupled problem, dispersion is the key to understanding the wave-induced stress felt by ice.

Theoretically, wave dispersion in ice is related to the mechanical model of ice. Ice mechanics manifest in the dispersion relation as extra terms including mass loading which shortens the wavelength, elasticity (or flexural-rigidity) which increases the wavelength, effective viscosity of a layer which increases wavelength (à la Keller 1998), and dissipation in the viscoelastic EFS model which is neutral to wavelength. The net result, shortening or lengthening, depends on the specific combination of ice properties and frequency in question. Snell's law gives refraction (change in wave direction) and change in wavelength which leads to shoaling (change in wave height) through conservation of momentum. Observations were compiled and interpreted in the context of these theoretical concepts of dispersion.

Actual measurements of the dispersion relation are rare in the literature. An overall picture starts to emerge when considering the combined results from the individual case studies as summarized in Table 1. Loose pancake ice in the MIZ does not have elastic properties (see Fig. 8), and often a shortened wavelength (Wadhams and Holt 1991; Wadhams et al. 2002; De Carolis 2003; this study) was reported. Mass loading is almost certainly the cause of the shortening although inverting the ML model ends in an overestimation of ice thickness, so viscous-layer models have also been applied here (Wadhams et al. 2002). Conceptually, as the pancakes become compact or compressed, or the frazil/brash matrix between pancakes becomes substantial, viscosity and elasticity could start to play a role. The literature presents mixed results with both lengthening and shortening observed (Liu et al. 1991; Fox and Haskell 2001; Wadhams et al. 2004); note, this is not necessarily inconsistent with the models, indeed Liu et al. (1991) matched a viscoelastic model to their results, however, dispersion under these ice conditions is not well understood. Observations of waves on the Arctic interior ice and on fast ice are generally consistent with the flexural-gravity model (Squire and Allan 1977; Marsan et al. 2012; Sutherland and Rabault 2016) and quantitative matches have been found. Remarkably, Sutherland and Rabault (2016) observed a transition to the open water relation as the ice sheet fractured, presumably losing its elasticity.

However, the whole empirical body of literature is a series of case studies, each of which fall well short of giving a comprehensive picture some with contradictory results. A number of potential problems with the empirical studies are discussed, including the lack of colocated measurements of surface currents, the gradient of which also causes deviation from linear dispersion. Many of these problems could be circumvented in the future by utilizing a spatiotemporal measurement technique. Nevertheless, a definitive measurement will be difficult because of the inherent tradeoff between signal strength and the signature of dispersion. Just as the problem of wave-ice interaction is highly coupled, the way forward must include progress in our understanding of both waves and their icy medium.

Acknowledgements COC was supported by an ASEE postdoctoral fellowship and a Karles fellowship at NRL. Discussions with A. Marchenko (University Center in Svalbard), A. Babanin (University of Melbourne), and a presentation by W. Perrie (Bedford Institute of Oceanography) motivated this paper. The comments of J. Mosig and V. Squire (University of Otago) greatly improved an early version of this manuscript. We are additionally grateful to V. Squire who supplied a code for the EFS model. We also acknowledge clarifying discussions with P. Wadhams (Cambridge University) and H. Shen (Clarkson University). We thank Editor O. Breivik and the two anonymous reviewers for their diligence and patience through multiple revisions which lead to a substantially improved manuscript.

References

Ardhuin, F., F. Collard, B. Chapron, F. Girard-Ardhuin, G. Guitton, A. Mouche, and J. Stopa 2015. Estimates of ocean wave heights and attenuation in sea ice using the SAR wave mode on Sentinel-1A. Geophys. Res. Lett

Ardhuin, F., P. Sutherland, M. Doble, and P. Wadhams (2016a), Ocean waves across the Arctic: Attenuation due to dissipation dominates over scattering for periods longer than 19 s, Geophys. Res. Lett., 43, 5775-5783

Ardhuin F., B. Chapron, F. Collard, M. Smith, J.E. Stopa, J. Thomson, M. Doble, B. Blomquist, O. Persson, C.O. Collins III, & P. Wadhams (2016b) Measuring ocean waves in sea ice using SAR imagery: A quasi-deterministic approach evaluated with Sentinel-1 and in situ data. doi:10.1016/j.rse.2016.11.024

Asplin, M. G., R. Galley, D. G. Barber, and S. Prinsenberg (2012), Fracture of summer perennial sea ice by ocean swell as a result of Arctic storms, J Geophys Res: Oceans, 117(C6), 2156 - 2202.

Asplin MG, Scharien R, Else B, Howell S, Barber DG, Papakyriakou T, Prinsenberg S (2014) Implications of fractured Arctic perennial ice cover on thermodynamic and dynamic sea ice processes. Journal of Geophysical Research: Oceans 119(4):2327–2343

Borge JCN, Reichert K, Dittmer J (1999) Use of nautical radar as a wave monitoring instrument. Coast Eng 37(3–4):331–342

Broström, G. and K. Christensen (2008), Waves in sea ice. Report 5/2008, Nor Meteorol Inst., http://met.no/Publikasjoner+2008.b7C_wlfY47.ips

Campbell AJ, Bechle AJ, Wu CH (2014) Observations of surface waves interacting with ice using stereo imaging. Journal of Geophysical Research: Oceans 119(6):3266–3284

Collins CO III, Lund B, Ramos RJ, Drennan WM, Graber HC (2014) Wave measurement intercomparison and platform evaluation during the ITOP (2010) experiment. J Atmos Ocean Technol 31(10):2309–2329

Collins III, C. O., W. E. Rogers, A. Marchenko, and A. V. Babanin (2015), In situ measurements of an energetic wave event in the Arctic marginal ice zone, Geophys. Res. Lett.

Collins III, C. O., W. E. Rogers, & A. Marchenko (2016) On wave-ice interaction in the Arctic marginal ice zone: dispersion, attenuation, and ice response (No. NRL/MR/7320—16-9676). Naval Research Lab, Stennis Space Center, MS 39529–5004.

Dalrymple RA, Liu PL-F (1978) Waves over soft muds: a two-layer fluid model. J Phys Oc 8:1121–1131

Dean RG, Dalrymple RA (1991) Water wave mechanics for engineers and scientists. World Scientific, Hackensack, NJ, USA. pp. 353

De Carolis, G. (2003), March. SAR observations of waves in ice. In *International Symposium on Remote Sensing* (pp. 141–151). International Society for Optics and Photonics.

De Carolis G, Desiderio D (2002) Dispersion and attenuation of gravity waves in ice: a two-layer viscous fluid model with experimental data validation. Phys Lett A 305(6):399–412

Doble MJ, Bidlot J (2013) Wave buoy measurements at the Antarctic sea ice edge compared with an enhanced ECMWF WAM: progress towards global waves-in-ice modelling. Ocean Model 70:166–173

Ewing M, Crary AP (1934) Propagation of elastic waves in ice. Part II. J Appl Phys 5(7):181–184

Fox C, Haskell TG (2001) Ocean wave speed in the Antarctic marginal ice zone. Ann Glaciol 33(1):350–354

Fox C, Squire VA (1994) On the oblique reflexion and transmission of ocean waves at shore fast sea ice, philosophical transactions of the Royal Society of London. Series A: Physical and Engineering Sciences 347(1682):185–218

Horvat C, Tziperman E (2015) A prognostic model of the sea-ice floe size and thickness distribution. Cryosphere 9(6):2119–2134

Keller JB (1998) Gravity waves on ice-covered water. Journal of Geophysical Research: Oceans 103(C4):7663–7669

Keller JB, Weitz M (1953) Reflection and transmission coefficients for waves entering or leaving an icefield. Communications on Pure and Applied Mathematics 6(3):415–417

Kinsman B (1965) Wind waves, their generation and propagation on the ocean surface. Prentice-Hall, Englewood Cliffs

Kirby, J., (1992), Water waves in variable depth under continuous sea ice, Proceedings of the Second International Conference on Offshore and Polar Engineering Conference, San Francisco, USA, 14–19 June.

Kohout AL, Meylan MH (2008) An elastic plate model for wave attenuation and ice floe breaking in the marginal ice zone. Journal of Geophysical Research 113(C9)

Kohout AL, Williams M, Dean S, Meylan MH (2014) Storm-induced sea-ice breakup and the implications for ice extent. Nature 509(7502):604–607

Kohout, A., M. Williams, T. Toyota, J. Lieser, and J. Hutchings (2015), In situ observations of wave-induced sea ice breakup, Deep Sea Research Part II: Topical Studies in Oceanography.

Krogstad HE, Trulsen K (2010) Interpretations and observations of ocean wave spectra. Ocean Dyn 60(4):973–991

Kuik AJ, Van Vledder GP, Holthuijsen LH (1988) A method for the routine analysis of pitch-and-roll buoy wave data. J Phys Oceanogr 18(7):1020–1034

Leckler F, Ardhuin F, Peureux C, Benetazzo A, Bergamasco F, Dulov V (2015) Analysis and interpretation of frequency–wavenumber spectra of young wind waves. J Phys Oceanogr 45(10):2484–2496

Liu AK, Mollo-Christensen E (1988) Wave propagation in a solid ice pack. J Phys Oceanogr 18(11):1702–1712

Liu AK, Holt B, Vachon PW (1991) Wave propagation in the marginal ice zone: model predictions and comparisons with buoy and synthetic aperture radar data. Journal of Geophysical Research: Oceans 96(C3):4605–4621

Long RB (1980) The statistical evaluation of directional spectrum estimates derived from pitch/roll buoy data. J Phys Oceanogr 10(6): 944–952

Longuet-Higgins, M. S., D. E. Cartwright, and N. D. Smith (1963), Observations of the directional spectrum of sea waves using the motions of a floating buoy *Ocean Wave Spectra* Prentice-Hall, 111–136.

Lund B, Collins CO, Graber HC, Terrill E, Herbers TH (2014) Marine radar ocean wave retrieval's dependency on range and azimuth. Ocean Dyn 64(7):999–1018

Lund B, Graber HC, Hessner K, Williams NJ (2015) On shipboard marine X-band radar near-surface current "Calibration". J Atmos Ocean Technol 32(10):1928–1944

Marsan D, Weiss J, Larose E, Métaxian JP (2012) Sea-ice thickness measurement based on the dispersion of ice swell. The Journal of the Acoustical Society of America 131(1):80–91

Meylan MH, Squire VA (1995) The response of a thick flexible raft to ocean waves. Int J of Offshore and Polar Eng 5(3):198–203

Mindlin RD (1951) Influence of rotatory inertia and shear on flexural motion of isotropic elastic plates. Transactions of the American Society of Mechanical Engineering: Journal of Applied Mechanics 18:31–38

Mosig, J. E., F. Montiel, and V. A. Squire (2015), Comparison of viscoelastic-type models for ocean wave attenuation in ice-covered seas, J Geophys Res: Oceans

Newyear K, Martin S (1999) Comparison of laboratory data with a viscous two-layer model of wave propagation in grease ice. Journal of Geophysical Research: Oceans 104(C4):7837–7840

Robinson NJ, Palmer SC (1990) A modal analysis of a rectangular plate floating on an incompressible liquid. J Sound Vib 142(3):453–460

Rogers, W. E. and S. S. Zieger (2014), S_{ice}: Damping by sea ice, in User manual and system documentation of WAVEWATCH III(R) version 4.18b,, edited by H. L. Tolman, pp. 60–61, College Park, MD, Tech. Note, MMAB Contribution 316 NOAA/NWS.

Sakai, S. and K. Hanai (2002), Empirical formula of dispersion relation of waves in sea ice, paper presented at Ice in the environment: Proceedings of the 16th IAHR International Symposium on Ice.

Shuchman RA, Rufenach CL, Johannessen OM (1994) Extraction of marginal-ice-zone thickness using gravity wave imagery. Journal of Geophysical Research: Oceans 99(C1):901–918

Snodgrass FE, Groves GW, Hasselmann KF, Miller GR, Munk WH, Powers WH (1966) Propagation of ocean swell across the Pacific. Philosophical Transactions of the Royal Society of London A: Mathematical, Physical and Engineering Sciences 259(1103):431–497

Squire VA, Moore SC (1980) Direct measurement of the attenuation of ocean waves by pack ice. Nature 283 (5745):365–368

Squire VA (1993) A comparison of the mass-loading and elastic plate models of an ice field. Cold Reg Sci Technol 21(3):219–229

Squire VA (2007) Of ocean waves and sea-ice revisited. Cold Reg Sci Technol 49(2):110–133

Squire, V.A. and A. Allan (1977), Propagation of flexural gravity waves in sea ice. Centre for Cold Ocean Resources Engineering, Memorial University of Newfoundland

Squire VA, Dugan JP, Wadhams P, Rottier PJ, Liu AK (1995) Of ocean waves and sea ice. Annu Rev Fluid Mech 27(1):115–168

Stein PJ, Euerle SE, Parinella JC (1998) Inversion of pack ice elastic wave data to obtain ice physical properties. Journal of Geophysical Research: Oceans 103(C10):21783–21793

Sutherland G, Rabault J (2016) Observations of wave dispersion and attenuation in landfast ice. Journal of Geophysical Research: Oceans 121(3):1984–1997

Tabata, T. (1958), Studies on visco-elastic properties of sea ice. Arctic Sea Ice, pp. 139–147, Proceedings of the Arctic Sea Ice Conference, Easton Maryland, 1958

Thomson J, Rogers WE (2014) Swell and sea in the emerging Arctic Ocean. Geophys Res Lett 41(9):3136–3140

Thomson, J., V. Squire, S. Ackley, E. Rogers, A. Babanin, P. Guest, T. Maksym, P. Wadhams, S. Stammerjohn, and C. Fairall (2013), Sea state and boundary layer physics of the emerging arctic ocean (No. APL-UW-1306). University of Washington Technical Document

Thomson J, Talbert J, de Klerk A, Brown A, Schwendeman M, Goldsmith J, Thomas J, Olfe C, Cameron G, Meinig C (2015) Biofouling effects on the response of a wave measurement buoy in deep water. J Atmos Ocean Technol 32(6):1281–1286

Thomson, J., Y. Fan, S. Stammerjohn, J. Stopa, W.E. Rogers, F. Girard-Ardhuin, F. Ardhuin, H. Shen, W. Perrie, H. Shen, S. Ackley, A. Babanin, Qi. Liu, P. Guest, T. Maksym, P. Wadhams, C. Fairall, O. Persson, M. Doble, H. Graber, B. Lund, V. Squire, J. Gemmrich, S. Lehner, B. Holt, M. Meylan, J. Brozena, J.-R. Bidlot, 2016, Emerging trends in the sea state of the Beaufort and Chukchi Seas. Ocean Modelling. doi:10.1016/j.ocemod.2016.02.009

Timco GW, Weeks WF (2010) A review of the engineering properties of sea ice. Cold Reg Sci Technol 60(2):107–129

Toffoli A, Waseda T, Houtani H, Cavaleri L, Greaves D, Onorato M (2015) Rogue waves in opposing currents: an experimental study on deterministic and stochastic wave trains. J Fluid Mech 769:277–297

Tolman, H. L. and the WAVEWATCH III® Development Group (2014), User Manual and System Documentation of WAVEWATCH III® version 4.18, tech. note 316, NOAA/NWS/NCEP/MMAB

Tucker MJ (1989) Interpreting directional data from large pitch-roll-heave buoys. Ocean Eng 16(2):173–192

Tucker, M.J. and Pitt, E.G., 2001. Waves in ocean engineering (No. Volume 5).

Wadhams P (2000) Ice in the ocean. CRC Press

Wadhams P, Doble M (2009) Sea ice thickness measurements using episodic infragravity waves from distant storms. Cold Regions Sci Technol 56:98–101

Wadhams P, Holt B (1991) Waves in frazil and pancake ice and their detection in Seasat synthetic aperture radar imagery. Journal of Geophysical Research: Oceans 96(C5):8835–8852

Wadhams P, Parmiggiani FF, De Carolis G (2002) The use of SAR to measure ocean wave dispersion in frazil-pancake icefields. J Phys Oceanogr 32(6):1721–1746

Wadhams P, Parmiggiani FF, De Carolis G, Desiderio D, Doble MJ (2004) SAR imaging of wave dispersion in Antarctic pancake ice and its use in measuring ice thickness. Geophys Res Lett 31(15)

Wadhams P, Squire VA, Goodman DJ, Cowan AM, Moore SC, (1988) The attenuation rates of ocean waves in the marginal ice zone. Journal of Geophysical Research 93(C6):6799

Wang R, Shen HH (2010a) Gravity waves propagating into an ice-covered ocean: a viscoelastic model. Journal of Geophysical Research: Oceans 115(C6)

Wang R, Shen HH (2010b) Experimental study on surface wave propagating through a grease–pancake ice mixture. Cold Reg Sci Technol 61(2):90–96

Weber JE (1987) Wave attenuation and wave drift in the marginal ice zone. J Phys Oceanogr 17(12):2351–2361

Weitz, M. and J. B. Keller (1950), Reflection of water waves from floating ice in water of finite

Whitham GB (2011) Linear and nonlinear waves, vol. 42. John Wiley & Sons, NY, pp. 636. doi:10.1002/9781118032954

Williams TD, Bennetts LG, Squire VA, Dumont D, Bertino L (2013a) Wave–ice interactions in the marginal ice zone. Part 1: theoretical foundations. Ocean Model 71:81–91

Williams TD, Bennetts LG, Squire VA, Dumont D, Bertino L (2013b) Wave–ice interactions in the marginal ice zone. Part 2: numerical implementation and sensitivity studies along 1D transects of the ocean surface. Ocean Model 71:92–101

Young IR, Rosenthal W, Ziemer F (1985) A three-dimensional analysis of marine radar images for the determination of ocean wave directionality and surface currents. Journal of Geophysical Research: Oceans 90(C1):1049–1059

Zhang, B., W. Perrie, and Y. He (2010), Validation of RADARSAT-2 fully polarimetric SAR measurements of ocean surface waves. Journal of Geophysical Research: Oceans (1978–2012) 115.C6.

Zhao X, Shen HH, Cheng S (2015) Modeling ocean wave propagation under sea ice covers. Acta Mech Sinica 31(1):1–15